The Mek1 phosphorylation cascade plays a role in meioticrecombination of *Schizosaccharomyces pombe*

Takahiro Tougan [1], Takashi Kasama [1], Ayami Ohtaka [1], Daisuke Okuzaki [1], Takamune T. Saito [1, 3], Paul Russell [3], and Hiroshi Nojima [1, 4]

Supplementary Data

Supplementary Results

The *mek1-T15A* mutation causes a delay in the initiation of meiotic S phase. To identify the physiological consequence of T15 phosphorylation of Mek1, we constructed a mutant in which the *mek1*$^+$ gene is replaced by the *mek1-T15A-9myc* allele and expressed by the *mek1*$^+$ promoter. We previously showed that the timing of meiotic progression of *mek1Δ* cells is the same as that of WT cells (Shimada et al., 2002)[23].[23] The effect of the T15A mutation on the timing of meiotic progression was assessed by monitoring the meiotic progression profiles of *mek1-T15A-9myc pat1* cells. The *pat1-114* temperature-sensitive strain mutation was included because it causes cells to enter meiosis in a highly synchronous manner when they are shifted to the inductive temperature. Thus, homozygous diploid *mek1-9myc pat1* cells, or *mek1-T15A-9myc pat1* cells, were arrested in G_1 phase by nitrogen starvation and then shifted to the inductive temperature to induce synchronous meiosis. The number of nuclei in the cells of the *mek1*$^+$ intact strain, *mek1-9myc pat1*, was quantified over time. The frequency of two-nuclei cells peaked 5.0 h after meiotic induction (Fig. 3A, left panel). This profile is also similar to that of *mek1*$^+$ *pat1* cells (data not shown). In contrast, the number of *mek1-T15A-9myc pat1* cells with two nuclei peaked at 6.0 h, a 1-h delay in meiotic progression compared to that of *mek1*$^+$ cells (Fig. 3A, right panel).

Time course FACS analysis was then used to follow the progression of the meiotic S-phase to determine at what point *mek1-T15A-9myc pat1* cells become delayed. This analysis showed that the initiation of meiotic S phase was delayed in *mek1-T15A-9myc pat1* cells as compared to *mek1-9myc pat1* cells (Fig. 3B, upper panels). The FACS data was analyzed with Modfit LT software (BD Biosciences, Franklin Lakes, NJ) to determine the frequency of cells in the meiotic S phase. As shown in Figure 3B (lower panels), *mek1-9myc pat1* cells at meiotic S phase peak at 2.0 h, whereas *mek1-T15A-9myc*

pat1 cells peak at 3.0 h. Moreover, DNA replication peaked at 2.0 h in *mek1-9myc pat1* cells, although it had not yet started in *mek1-T15A-9myc pat1* cells (Fig. 3B, lower right panel, gray arrowhead). These results demonstrate that the *T15A* mutation caused a 1-h delay in the initiation of meiotic S phase.

Next, the expression and degradation profiles of the Mek1 and Mek1-T15A proteins were investigated by western blot analysis. The two proteins appeared at the same time, but Mek1 degradation was delayed by 1 h in *mek1-T15A-9myc pat1* cells relative to *mek1-T15A-9myc pat1* cells (Fig. 3C), suggesting that Mek1 is retained 1 h longer during meiosis in *mek1-T15A-9myc pat1* cells. We previously showed that the meiotic delay caused by the meiotic recombination checkpoint is linked to the phosphorylation of Tyr15 of Cdc2 (Saito et al., 2004).[36] To determine whether the Mek1-T15A meiotic delay is linked to this same phosphorylation event, we monitored the phosphorylation of Cdc2 Tyr15 during meiosis. As shown in Figure 3C (lower panels), phosphorylated Cdc2 as detected by the anti-Cdc2-Tyr15 antibody appeared and disappeared with a 1-h delay in *mek1-T15A-9myc pat1* cells as compared to its lifespan in *mek1-9myc pat1* cells, consistent with the length of the delay in the onset of meiotic division in *mek1-T15A-9myc pat1* cells. These results suggest that the 1-h delay in the two-nucleus peak in *mek1-T15A-9myc pat1* cells (Fig. 3A) is due to the delay in meiotic S phase resulting from the altered degradation of Mek1.

The *mek1-KD* mutation does not affect meiotic progression. To understand the role of the kinase activity of Mek1 in meiotic progression, we constructed a site-specific mutant (*mek1-KD-9myc*) bearing point mutations designed to destroy its kinase activity (Fig. 1A). We confirmed that the D281A mutation abolishes Mek1 kinase activity (Fig. S3A). Two-nucleus *mek1-KD-9myc pat1* cells peak at 4.5 h, which is slightly earlier than the two-nucleus peak of *mek1*$^+$ cells at 5.0 h (Fig. S3B). The peak of cell numbers at meiotic S phase (2.0 h) is also similar to that of *mek1*$^+$ cells (Fig. S3C, left panels). The peak meiotic frequencies of *mek1-T15A/KD-9myc pat1* cells with two nuclei (5.0 h) or atmeiotic S phase (2.5 h) are similar to those of *mek1*$^+$ cells (Figures S3B and S3C, right panels). Western blots showed that the temporal profiles of Mek1 protein levels and Tyr15 phosphorylation of Cdc2 are similar to those of *mek1*$^+$ cells (Fig. S3D). These results are consistent with the onset of meiosis I chromosome segregation in these mutant cells (Fig. S3B). They also indicate that the delay in the initiation of meiotic S phase in *mek1-T15A-9myc pat1* cells is suppressed by the KD mutation.

The *mek1-FHAD* mutation causes a slight delay in meiotic progression.

A mutant bearing inactivating point mutations in the FHA domain was constructed to evaluate the role of this domain in meiotic progression (Fig. 1A). During meiotic progression, the frequency of *mek1-FHAD-9myc pat1* cells with two nuclei peaked at 5.5 h (Fig. S5A, left panel), a slight delay (30 min) compared to the *mek1*$^+$ (*mek1-9myc pat1*) cell peak at 5.0 h (Fig. S5A). Two-nucleus *mek1-T15A/FHAD-9myc pat1* cells also peaked at 5.5 h (Fig. S5A, right panel), at the same time as *mek1-FHAD-9myc pat1* cells, and 30 min earlier than *mek1-T15A-9myc pat1* cells. Similarly, the meiotic S phase peak in *mek1-FHAD-9myc pat1* was at 2.5 h (Fig. S5A, left panels), which is also a slight delay (30 min) compared to that in *mek1*$^+$ cells, which peaked at 2.0 h (Fig. S5B). On the other hand, the meiotic S phase peak in *mek1-T15A/FHAD-9myc pat1* cells was at 2.5 h (Fig. S5B, right panels), again the same as that in *mek1-FHAD-9myc pat1* cells and 30 min earlier than in *mek1-T15A-9myc pat1* cells. These results indicate that the FHAD mutation causes a slight delay in the initiation of meiotic S phase and partially suppresses the meiotic delay of *mek1-T15A-9myc pat1* cells.

Western blots showed that the timing of Mek1 appearance and disappearance in *mek1-FHAD-9myc pat1* and *mek1-T15A/FHAD-9myc pat1* cells was also delayed, reflecting the delay in meiotic progression (Fig. S5C). The timing of phosphorylation of Cdc2 Tyr15 was also similar to that in *mek1-T15A-9myc pat1* cells, reflecting the meiotic delay.

The meiotic recombination frequency is reduced by the *FHAD* and *KD* mutations, but not by the *T15A* mutation. The effect of the *mek1* mutations on homologous recombination was investigated by measuring the rates of intergenic and intragenic recombination in *mek1-KD*, *mek1-FHAD* and *mek1-T15A* single mutant cells and in double mutant cells. Intergenic recombination (crossing-over) was monitored by measuring the genetic distance between *cdc12*$^+$ and *lys3*$^+$ on chromosome I. Intragenic recombination was measured with the *ade6* alleles *ade6-M26* and *ade6-469*. As shown in Figure S5A and B, the frequencies of both intergenic and intragenic recombination in *mek1Δ* cells were reduced and those of *mek1-KD-9myc* cells were modestly reduced. These results indicate that the kinase activity of Mek1 plays a role in meiotic recombination.

In contrast, the recombination frequencies of *mek1-FHAD-9myc* cells were less strongly reduced, to levels intermediate between those of *mek1*$^+$ and *mek1Δ* cells. The recombination frequencies of *mek1-T15A-9myc* cells were similar to those of wild-type cells, and the inclusion of the T15A mutation in *mek1-KD-9myc* and *mek1-FHAD-9myc* cells had no further effect on meiotic recombination in these mutants. These results

indicate that the phosphorylation of Thr15 plays no role in meiotic recombination. Analysis of the spore viability of mutant cells revealed no remarkable differences compared to wild-type cells (Fig. S6C).

Determination of phosphorylation sites on Mus81 by Mek1 and Cds1 *in vitro*. We explored to determine the phosphorylation sites of Mus81 by Mek1 and/or Cds1. We fist noticed that Mus81 has two RxxS/RxxT motifs at T218 and T422 that are expected to be preferentially phosphorylated by Chk2 kinase families such as Cds1 and Mek1 (Fig. S6A). To determine whether any of these motifs serve as a phosphorylation target of Mek1 and/or Cds1, we performed *in vitro* kinase assays using plasmids that express GST-fused *S. pombe* Mus81 fragments containing these putative target sites as substrates (Sub1 and Sub2 in Fig. S6A) using Mek1/AL (Figs. 4C and S6) or GST alone as a positive or negative control, respectively. To obtain Cds1 kinase activity, we prepared the immunoprecipitates of the cell extracts from logarithmically growing *S. pombe* cells that were exogenously expressing Cds1-2HA/6His proteins from the promoter of *cds1*$^{+}$ gene. We found that both Mek1 (Fig. S6B-i, lanes 10, 11 and 1) and Cds1 (Fig. S6B-ii, lanes 8, 10 and 13) phosphorylated the GST-Mus81 fragment containing T218 (Sub1) and T422 (Sub1) to a similar level to Mek1/AL (lane 1 in Fig. S6B-i and lane 13 in Fig. S6B-ii). In contrast, when we constructed T218A and T422A in which we replaced Thr218 and T422 by alanine, we found that the peptide fragment incorporated only negligible amounts of ^{32}P by both Mek1 (Fig. S6B-i, lanes 11 and 13) and Cds1 (Fig. S6B-ii, lanes 9 and 11). These results indicate that Thr218 and Thr422 of Mus81 are responsible for Mek1- and Cds1-dependent ^{32}P incorporation.

To determine whether Mus81 has other Mek1- and Cds1-dependent phosphorylation sites that do not include RxxS/RxxT motifs, we produced deletion mutants of Mus81 as GST-fusion proteins that covers the whole Mus81 molecule (Fig. S6A) and used them as substrates for *in vitro* kinase assays. We found that fragment 219-421 alone showed Mek1- and Cds1-dependent ^{32}P incorporation (arrows in lanes 10 of Fig. S6C-i and ii). It appears that Mek1 caused much less ^{32}P incorporations than Cds1 because the ratios of band intensities between fragment 219-421 and GST-Sub1 (or GST-Sub2) are much smaller in Mek1 than Cds1 (see arrows and arrowheads in Fig. S6C). We next dissected it into several fragments and found that the fragment 252-362 (lanes 9 of Fig. S6D-i and ii) alone showed ^{32}P incorporation to a similar level of fragment 219-421 (lanes 7 of Fig. S6D-i and ii). The ratio of band intensity between fragment 252-362 and GST-Sub1 (lanes 12 of Fig. S6D-i and ii) is also much smaller in Mek1 than Cds1 (see arrows and arrowheads in Fig. S6D). Further dissection of this band into three revealed that the

fragment 252-313 alone showed Mek1- and Cds1-dependent ^{32}P incorporation (arrows in lanes 10 of Fig. S6E-i and ii). Finally, since this fragment contained three possible target sites of phosphorylations, we prepared GST-fusion proteins that harbor replacements of these sites into alanine (T260A , S270A and T275A) for *in vitro* kinase assays. We found that, whereas phosphorylation of the T260A, S270A mutants was not significantly altered, the phosphorylation of the T275A mutant was remarkably diminished (see small arrows in lanes 12 in Fig.S6F-1 and ii). We also confirmed that triple alanine mutant protein (3A) that harbor alanine replacements in all of these sites also abolished Mek1- and Cds1-dependent ^{32}P incorporation (lanes 13 of Fig. S6C-i and ii). We also confirmed in loading control experiments with Simply Blue (SB) staining that an equal amount of each protein had been applied (left panels of Fig. S6A-F). These results indicate that Mek1 than Cds1phosphorylate Mus81 at T218, T275 and T422 *in vitro*.

The *rdh54*$^+$ gene is predominantly expressed during early meiosis. The *rdh54*$^+$ gene of *S. pombe* (Catlett et al., 2003),[28] an ortholog of *S. cerevisiae RDH54* (43), is a meiosis-specific gene, as its transcript (3.3 kb) appears only during meiosis (Fig. S9A, i). In this experiment, we took advantage of the fact that, upon nitrogen starvation, the heterozygous CD16-1 (h^+/h^-) strain initiates meiosis, while the homozygous CD16-5 (h^-/h^-) strain does not. By northern blot analysis, we hybridized RNA from these strains with a probe that spanned the protein-coding region of *rdh54*$^+$. We also confirmed that meiosis was induced upon nitrogen starvation by counting the frequency of cells with 1, 2, 3, or 4 nuclei at 2-h intervals by fluorescence microscopy (Fig. S9A, ii).

The termination codon of the neighboring *atf31*$^+$, a meiosis-specific transcription factor gene, is only 15 bases away from the termination codon of *rdh54*$^+$ (Fig. S9A, iii). Consequently, it appears that the *rdh54*$^+$ probe used here also detected the *atf31*$^+$ gene transcript (1.3 kb), whose sequence overlaps with that of *rdh54*$^+$ (Fig. S9A, i). The *rdh54*$^+$ and *atf31*$^+$ transcripts displayed a similar expression pattern, in that expression levels peaked at the horsetail phase and in early meiosis I (8 h after induction), which is when homologous chromosome pairing and recombination occur. Consequently, we were concerned that if we disrupted the *rdh54*$^+$ gene that this might also disrupt the 3' non-coding region of *atf31*$^+$ gene and thereby affect its expression. To avoid this possibility, we deleted about 70% of the *rdh54*$^+$ gene (from the initiation codon through exon 12) in our *rdh54*Δ strain (Fig. S9A, iii). This was expected to abolish the expression of Rdh54 while leaving the majority of the 3' non-coding region of the *atf31*$^+$ gene intact.

Indeed, *rdh54*Δ diploid cells seemed to lack a functional Rdh54 protein because they failed to repair the DSBs caused by MMS, and they were more sensitive to the drug as

compared to WT cells during the vegetative cell cycle (Fig. S9B, i). This phenotype is expected based on a previous report (Catlett et al., 2003).[28] In contrast, *rdh54*Δ haploid cells are not sensitive to MMS during the vegetative cell cycle (Fig. S9B, ii). Furthermore, the additional elimination of *rhp54*$^{+}$, an *S. pombe* paralog of *rdh54*$^{+}$, did not increase MMS sensitivity relative to that of single mutant *rhp54Δ* cells (Fig. S9B, ii). Moreover, although *rhp54Δ* cells showed mitotic growth defects, *rdh54*Δ cells did not, and *rdh54Δ rhp54Δ* double mutant cells showed mitotic defects similar to that of *rhp54Δ* cells (data not shown). These results indicate that *rdh54*$^{+}$ does not participate in DNA damage repair during the haploid vegetative cell cycle (9).

RNA was extracted from meiotic *rdh54*Δ cells, and northern blot analysis using an *atf31*$^{+}$-specific probe indicated that *atf31*$^{+}$ expression is not affected in our *rdh54*Δ cells (Fig. S9C). The delay of the peak of *atf31*$^{+}$ expression is due to a delay in the meiotic progression of *rdh54*Δ cells (Fig. S9C, i). Thus, the phenotypes described below using the *rdh54*Δ cells are considered to be due to the disruption of Rdh54, but not Atf31.

Rdh54 forms nuclear foci during the horsetail phase. To determine the subcellular localization of Rdh54 during meiosis, we prepared an Rdh54-GFP-expressing strain in the h^{90} genetic background. Nuclei were stained with Hoechst33342, and Rdh54-GFP was imaged in live cells after meiotic induction. The Rdh54-GFP signal was detected in the nucleus from the horsetail phase to meiosis II (Fig. S9D). Notably, the Rdh54-GFP signal appeared as multiple nuclear foci (dots) during the horsetail phase when HR occurs (horsetail panel in Fig. S9D). In parallel, we confirmed that Rdh54-GFP was expressed with a timing similar to that of *rdh54*$^{+}$ (see Fig. S9A-i) by performing a time-course western blot analysis (Fig. S9E). Moreover, we also confirmed that the Rdh54-GFP strain was not defective in HR rates or spore viability (see Fig. 6G), which indicates that Rdh54-GFP retains the activity of intact Rdh54.

Abnormal nuclear division of *rdh54Δ* cells during meiosis I. Observation of the nuclear division of *rdh54*Δ cells during meiosis I by microscopy (Fig. S10A, i) revealed cells with an abnormal nuclear morphology that is not observed in WT cells (Fig. S10A, ii). The percentage of cells displaying these abnormal nuclear shapes decreased as meiosis proceeded: 11.8, 8.9, and 1.1% of the cells were abnormal 5, 6 and 8 h after nitrogen starvation, respectively.

To determine the reason behind this defect, we examined when these abnormal nuclei appeared during meiosis and found that they appeared 15 minutes before the percentage of cells with two nuclei peaked (Fig. S10B). Moreover, when we compared

the behavior of spindles and nuclei in *rdh54*Δ cells by staining with an anti-α-tubulin antibody and Hoechst 33342, respectively, we found that a proportion of the nuclei failed to separate (Fig. S10C, left panels) and that the spindles were also slightly abnormal since their images were blurred. These results indicate that these aberrations occurred during meiosis I.

To further investigate the dynamic behavior of the nuclei in these abnormal *rdh54Δ* cells, we stained the cells with Hoechst 33342 to visualize the nucleus and the images were stored as a file that can be run as an animation on the internet. Several time-lapse images of a cell passing through meiosis I were taken at 2-min intervals and are shown in Figure S10D. It is apparent that meiosis I is prolonged in these abnormal *rdh54Δ* cells, as it takes 40 minutes for these cells to complete meiosis I as compared to 18 minutes for WT cells. However, the events that lead to the separation of the two nuclei, namely metaphase I, anaphase I and telophase I, proceeded with normal timing (18 min) in *rdh54Δ* cells. Moreover, compared to the WT nucleus, it appears as if the separation of all of the components of the nucleus is retarded in *rdh54Δ* cells as many granule-like structures appeared between the separating nuclei from 4 to 14 min. Furthermore, from 16 to 22 min, residual non-separated DNA persisted in these abnormal *rdh54Δ* cells. Nonetheless, at 40 min, all of the nuclear components appeared to have finally separated.

Notably, this prolonged separation and abnormal nuclear morphology was not observed in *rdh54Δ* cells during meiosis II, which indicates that this irregularity is specific to meiosis I (data not shown).

Supplementary Experimental Procedures

Protein extraction and western blotting. Protein extracts were prepared as previously described (Saito et al., 2003).[36] For Mek1-9myc detection, the blots were probed with the mouse monoclonal antibody 9E10 (Upstate Biotechnology) and, as a loading control, α-tubulin was detected with an anti-tubulin antibody (Sigma T5168). For detecting Cdc2 Tyr15 phosphorylation, the blots were probed with an anti-phospho-Cdc2 (Tyr15) rabbit polyclonal antibody (NEB 9111). To detect Cdc2 as a loading control, the anti-PSTAIRE antibody (Santa Cruz Biotechnology, Santa Cruz, CA) was used.

Recombination frequency and spore viability. Crossing-over rates were determined as previously described (Saito et al., 2003).[36] Briefly, haploid parental strains were grown on YPD plates at 30°C, and cells were mated and sporulated on ME plates at 28°C (zygotic meiosis). After 1 d of incubation, the spores were isolated. The frequency

of crossing-over was determined by measuring the genetic distance between *his2*$^+$ and *leu1*$^+$. The gene conversion rate was determined as previously described. For this, haploid parental strains were grown on YPD at 33°C. Cells were mated and sporulated on ME plates at 28°C (zygotic meiosis). After 2 d of incubation, the spores were treated with 1% glusulase (NEN Life Sciences, Perkin-Elmer, Boston, MA) for 2–3 h at room temperature and checked under a microscope for the complete digestion of contaminating vegetative cells. The glusulase-treated spores were washed with water, and the gene conversion rate and spore viability were measured. The frequency of gene conversion was determined with the *ade6-M26* and *ade6-469* alleles, as gene conversion between these alleles produces the *ade6*$^+$ allele.

***In vitro* kinase assays.** GST-Rad3 was expressed from a plasmid carrying the *nmt1* promoter, while the Mek1-T318A-9Myc, Mek1-T322A-9Myc, Mek1-T318AT322A-9Myc and Mek1-D281A(KD)-9Myc mutants were expressed from plasmids harboring the *nmt41* promoter. Tel1-GFP or Cds1-2HA/6His was expressed from the *tel1*$^+$ or *cds1*$^+$ genomic promoter, respectively. For immunoprecipitation, logarithmically growing cells (approximately 5×10^6 cells/mL) expressing each exogenously expressed protein were harvested. Cells were disrupted with glass beads in lysis buffer (50 mM Tris-HCl [pH 8.0], 150 mM NaCl, 10% glycerol, 1% NP-40, 50 mM NaF, 1 mM Na_3VO_4, 100 µg/mL PMSF, 1 µg/mL aprotinin, 1 µg/mL pepstatin, 1 µg/mL leupeptin, and 1 mM DTT) and centrifuged at 20,000 x *g* for 15 min at 4°C. Immune complexes were precipitated for GFP-, Myc-, or HA-fused kinases using rabbit polyclonal anti-GFP antibodies (MBL, Nagoya, Japan), mouse monoclonal antibody 9E10 (Upstate Biotechnology, Charlottesville, VA), mouse monoclonal antibody PL14 (MBL, Nagoya, Japan), or rat monoclonal antibody 3F10 (Roche, Basel, Switzerland). GST-fused Mek1 kinase and substrates were expressed in *E. coli*, which was disrupted by sonication in lysis buffer, and extracts were collected with Glutathione-Sepharose 4B (GE Healthcare, Uppsala, Sweden). Kinase assays were performed in kinase buffer (25 mM HEPES-KOH [pH 7.5], 50 mM KCl, 10 mM $MgCl_2$, 10 mM $MnCl_2$, 2% glycerol, 0.1% NP-40, 1 mM Na_3VO_4, and 1 mM DTT). To measure kinase activity, 5 µL of each kinase complex was added to a 25 µL reaction mixture containing 10 µM ATP, [γ-^{32}P] ATP and 15 µL of relevant substrates. Reactions were conducted at 30°C for 30 min and stopped by addition of 10 µL 4×SDS sample buffer and boiling. Samples were subjected to SDS-PAGE (10% gel) and visualized using the Bio-imaging Analyzer BAS 1800II (Fuji Film, Tokyo, Japan).

FACS analysis of DNA replication. Samples from meiotic cultures were pelleted and resuspended in 70% ethanol and stored at 4°C. Samples of 2–3 x 10^6 cells (3 mL) were aliquoted to new microtubes, pelleted, the ethanol removed, and the cells washed using 1 mL 50 mM Na-citrate. The supernatant was discarded and the pellet was resuspended in 0.5 mL 50 mM Na-citrate containing 0.1 mg/mL RNase A. These samples were incubated at 37°C for at least 2 h, and then 0.5 mL 50 mM Na-citrate containing 4 μg/mL propidium iodide (PI) was added. Samples were briefly sonicated and analyzed on a Becton-Dickinson FACScan.

Disruption of *rdh54*$^+$. The *rdh54*$^+$ gene in *S. pombe* was disrupted by replacing it with the *ura4*$^+$ cassette. PCR to obtain DNA fragments carrying the 5' upstream and 3' terminal regions of *rdh54*$^+$ was carried out with the following primers: rdh54-5F (5'-TAAACAAATCGCTCGG GGTACCGAGGATTCCAAAGCTTGTATGAGAAA-3'), rdh54-5R (5'-TTTCAATTCTT GCCGCTCGAGGTTCAGATTTCAGTTTTAATAAAGTAA-3'), rdh54-3F-2 (5'-GCGT GACGTCTGCAGCAAAAGCGGCCAGTCTGTATATACACATTTTTA-3'), and rdh54- 3R (5'-ATATCCGCTTTGCGAGCTCGCGGCCGCCGTTCGAACTTTTTATGCATT -3'). The underlined sequences denote artificially introduced restriction enzyme sites for *Kpn*I, *Xho*I, *Pst*I and *Sac*I, respectively. The *rdh54*$^+$ 5' upstream and 3' terminal PCR products and a 1.8-kb *Hin*dIII fragment containing the *ura4*$^+$ cassette (24, 34, 35) were inserted into the vector pBluescriptII KS(+) *via* the *Kpn*I-*Xho*I, *Pst*I-*Sac*I and *Hin*dIII sites, respectively. This plasmid construct was digested with *Pac*I and *Sac*I and introduced into the strain TP4-5A. Ura$^+$ transformants were screened by PCR and Southern blot analysis to identify the *rdh54*$^+$:: *ura4*$^+$ construct.

Construction of the *rhd54–gfp*$^+$ strain and *rhd54* mutants. To construct the strain that can express the Rdh54-GFP fusion protein, a DNA fragment carrying the 5' upstream region including native *rhd54*$^+$ promoter of the *rdh54*$^+$ gene fused to the open reading frame (ORF), and a fragment carrying the 3' downstream region of the *rdh54*$^+$ gene were amplified by PCR. The following oligonucleotides were synthesized and used as primers: for the *rdh54* 5' upstream-ORF region, rdh54-5F (5'-TAAACAAATCGCTCGGGGTACCGAGGATTCCAAAGCTTGTATGAGAAA-3') and rdh54-3R (5'-ATATCCGCTTTGCGAGCTCGCGGCCGCCGTTCGAACTTTTTATGCATT-3');

and for the *rdh54* 3' downstream region, rdh54-3UTR-F-XhoI (5'-ACGTCTCGAGTAGATCTATTTCGGACTTTTAAGG-3') and rdh54-SacI-R (5'-AAGCTTTAGAGCTCGGCGACGATCG-3'). The underlined sequences denote the artificially introduced restriction enzyme sites for *Kpn*I and *Not*I and for *Xho*I and *Sac*I, respectively. The 5' upstream-ORF and 3' downstream PCR products were inserted into the pUC19 vector *via* the *Kpn*I-*Not*I sites and into the pRGT1 vector *via* the *Xho*I-*Sac*I sites, respectively. Then, the 5' upstream-ORF fragment from the pUC19-rdh54-5'-ORF vector and the GFP-3' downstream fragment from the pRGT-rdh54-3' vector were inserted into the pIL(II) vector *via* the *Sal*I-*Not*I and *Not*I-*Sac*I sites, respectively. This construct (*rdh54-WT-GFP* construct; WT, wild type) was then digested with *Pac*I, and the resulting construct was introduced into the native *rdh54*$^{+}$ locus on the genome of the TK18-A (*rdh54Δ*) strain.

The *rdh54-T6A-GFP*, *rdh54-T158A-GFP*, *rdh54-T673A-GFP,* and *rdh54-K241R-GFP* strains were created by site-directed mutagenesis (Kunkel Method), using *rdh54-WT-GFP* construct as the template and the following oligonucleotides as primers: rdh54-T6A-F (5'-ATGAAACGAAGAGCGGCCTTTCAATGTCCATTAATTGAATC-3') and rdh54-T6A-R (5'-GATTCAATTAATGGACATTGAAAGGCCGCTCTTCGTTTCAT-3'); rdh54-T158A-F (5'-CAAGCCACCTTTGAGGCCTAACGCAATGTACCAGACAATATCAG-3') and rdh54-T158A-R (5'-CTGATATTGTCTGGTACATTGCGTTAGGCCTCAAAGGTGGCTTG-3'); rdh54-T673A-F (5'-CATTTTTATTCGCCAAAATGCTAAGCAAGGCCTTTCAAGTTCGTTC-3') and rdh54-T673A-R (5'-GAACGAACTTGAAAGGCCTTGCTTAGCATTTTGGCGAATAAAAATG-3'); and rdh54-K241R-F (5'-TTTTGGCTGATGAAATGGGCCTCGGCCGAACGTTGCAAACTATAACAGT-3') and rdh54-K241R-R (5'-ACTGTTATAGTTTGCAACGTTCGGCCGAGGCCCATTTCATCAGCCAAAA-3'), respectively. The underlined sequences denote the artificially introduced nucleotides that serve to replace threonine or lysine residues with alanine or arginine. These plasmid constructs were digested with *Pac*I, and the resulting construct was introduced into the native *rdh54*$^{+}$ locus on the genome of the TK18-A (*rdh54Δ*) strain.

Measurement of methylmethane sulfonate (MMS) sensitivity. Haploid yeast cells in the WT (TK20-HL), *rdh54rdh54Δ* (TK19-HL), *rhp54Δ* (TK27), and *rdh54Δrhp54Δ* background (TK30) were grown to mid-log phase in YPD. Diploid yeast cells in the WT (TK20-HL x TK20-W) and *rdh54Δ* background (TK19-HL x TK19-W) were grown to the mid-log phase in EMM-Ade medium. These cells were then plated on YPD in the presence or absence of MMS, and the plates were incubated at 30^{o}C for 4 d. MMS sensitivity was calculated as (the number of colonies on the plate at each MMS concentration)/(the number of colonies on the MMS-lacking plate) x 100.

Immunofluorescence. Meiotic cells were fixed with glutaraldehyde and paraformaldehyde (Saito et al., 2003).[36] The samples were then stained with 0.5 mg/ml Hoechst 33342 in PBS for 1 minute and mounted with antifade-containing Vectashield mounting medium (Vector Laboratories, Burlingame, CA). Fluorescence images of these cells were obtained by fluorescence microscopy (Axiophot, Zeiss, Germany or BX51, Olympus, Tokyo, Japan) with a charge-coupled device (CCD) camera (Photometrics PXL1400) or a Cool SNAP CCD camera (Roper Scientific, San Diego, CA). Immunofluorescence images were acquired using Adobe PhotoShop 6.0.

Fluorescent imaging of *rdh54Δ* chromosomes *in vivo*. Meiotic chromosomes were stained by inducing *pat1* (JZ670) and *pat1 rdh54Δ* cells (TK29) to enter meiosis by a temperature shift. The meiotic cells were stained with Hoechst 33342 (1.0 μg/ml) for a few minutes, mounted on a coverslip by spotting, and observed with a time-lapse microscope system. Images were taken with a 0.2 second exposure at 2-min intervals.

Table S1. Strains constructed and used in this study

Strain name	Genotype
CD16-1[a]	*h$^+$/h$^-$ ade6-M210/ade6-M216 cyh1/+ +/lys5-391*
CD16-5[a]	*h$^-$/h$^-$ ade6-M210/ade6-M216 cyh1/+ +/lys5-391*
TP4-5A[b]	*h$^-$ ade6-M210 leu1-32 ura4-D18*
TP4-1D[b]	*h$^+$ ade6-M216 his2 leu1-32 ura4-D18*
JZ670[c]	*h$^-$/h$^-$ ade6-M210/ade6-M216 leu1-32/leu1-32 pat1-114/pat1-114*
GP21	*h$^-$/h$^-$ ade6-M216/ade6-M210 leu1-32/leu1-32 ura4-D18/ura4-D18 mek1-KD-9myc::LEU2/mek1-KD-9myc::LEU2 pat1-114/pat1-114*
MS111-W1	*h$^+$ ade6-469 his2 leu1-32 ura4-D18*
MS105-1B	*h$^-$ ade6-M26 ura4-D18*
NB2118	*h$^+$ leu1-32 ura4-D18 cds1-2HA-6his::ura4$^+$*
NP32-2A	*h$^+$ his2 leu1-32 ura4-D18*
NP32-2B	*h$^-$ ura4-D18 cdc12ts lys3*
NP16-6B	*h$^-$ ade6-M216 ura4-D18*
TK18-A	*h$^-$ ade6-M210 leu1-32 ura4-D18 rdh54::ura4$^+$*
TK18-D	*h$^+$ ade6-M216 his2 leu1-32 ura4-D18 rdh54::ura4$^+$*
TK51-A	*h$^+$ ade6-M216 his2 leu1-32 ura4-D18 dmc1::ura4$^+$ rdh54::ura4$^+$*
TK51-D	*h$^+$ ade6-M216 his2 leu1-32 ura4-D18 dmc1::ura4$^+$ rdh54::ura4$^+$*
TK52-A	*h$^-$ ade6-M210 leu1-32 ura4-D18 dmc1::ura4$^+$*
TK52-D	*h$^+$ ade6-M216 his2 leu1-32 ura4-D18 dmc1::ura4$^+$*
Tk24-M26	*h$^-$ ade6-M26 ura4-D18*
TK24-469	*h$^+$ ade6-469 his2 leu1-32 ura4-D18*
TK23-M26	*h$^-$ ade6-M26 ura4-D18 rdh54$^+$::ura4$^+$*
TK23-469	*h$^+$ ade6-469 his2 leu1-32 ura4-D18 rdh54::ura4$^+$*
TK20-HL	*h$^+$ his2 leu1-32 ura4-D18*
TK20-W	*h$^-$ ura4-D18*
TK19-HL	*h$^+$ his2 leu1-32 ura4-D18 rdh54::ura4$^+$*
TK19-W	*h$^-$ ura4-D18 rdh54::ura4$^+$*
TK27	*h$^+$ his2 leu1-32 ura4-D18 rhp54::ura4$^+$*
TK30	*h$^+$ his2 leu1-32 ura4-D18 rdh54::ura4$^+$ rhp54::ura4$^+$*
TK29	*h$^-$/h$^-$ ade6-M210/ade6-M216 leu1-32/leu1-32 rdh54::ura4$^+$/rdh54::ura4$^+$ pat1-114/pat1-114*
TK118-WTG	*h^{90} leu1-32 ura4-D18 rdh54::rdh54-GFP-LEU2-ura4$^+$*
TK124-WT	*h$^-$/h$^-$ ade6-M210/ade6-M216 leu1-32/leu1-32 ura4-D18/ura4-D18 rdh54::rdh54-GFP-LEU2-ura4$^+$/rdh54::rdh54-GFP-LEU2-ura4$^+$ pat1-114/pat1-114*
TT77-GC-1	*h- ade6-M26 ura4-D18 hop1::ura4$^+$*

1	TT78-GC-1	*h^+ ade6-469 his2 ura4-D18 hop1::ura4$^+$*
2	TK118-T6A-1	*h^{90} leu1-32 ura4-D18 rdh541::rdh54-T6A-GFP-Leu2-ura4$^+$*
3	TK201-1	*h^{90} leu1-32 ura4-D18 rdh54::rdh54-T6A/T673A-GFP-LEU2-ura4$^+$*
4	TK118-K241R-1	*h^{90} leu1-32 ura4-D18 rdh54::rdh54-K241R-GFP-LEU2-ura4$^+$*
5	TK118-T6A/K241R-1	*h^{90} leu1-32 ura4-D18 rdh54::rdh54-T6A/K241R-GFP-LEU2-ura4$^+$*
6	TK123-1	*h^{90} leu1-32 ura4-D18 rdh54::rdh54-GFP-LEU2-ura4$^+$ mek1::ura4$^+$*
7	TT720	*h^- leu1-32 ura4-D18 tel1-GFP::LEU2*
8	TT623	*h^-/h^- ade6-M216/ade6-M210 leu1-32/leu1-32 ura4-D18/ura4-D18*
9		*mek1(100)-9myc::LEU2/mek1(100)-9myc::LEU2 pat1-114/pat1-114*
10	TT710	*h^-/h^- ade6-M216/ade6-M210 leu1-32/leu1-32 ura4-D18/ura4-D18*
11		*mek1-S12AS14AT15A(100)-9myc::LEU2/mek1-S12AS14AT15A (100)-9myc::LEU2 pat1-114/pat1-114*
12	TT705	*h^-/h^- ade6-M216/ade6-M210 leu1-32/leu1-32 ura4-D18/ura4-D18*
13		*mek1(100)-9myc::LEU2/mek1(100)-9myc::LEU2 rad3::ura4$^+$/rad3::ura4+ pat1-114/pat1-114*
14	TT286	*h^-/h^- ade6-M216/ade6-M210 leu1-32/leu1-32 ura4-D18/ura4-D18*
15		*mek1(100)-9myc::LEU2/mek1(100)-9myc::LEU2 tel1::ura4$^+$/tel1::ura4+ pat1-114/pat1-114*
16	TT201	*h^-/h^- ade6-M216/ade6-M210 leu1-32/leu1-32 ura4-D18/ura4-D18*
17		*mek1(100)-9myc::LEU2/mek1(100)-9myc::LEU2 rad3::ura4$^+$/rad3::ura4+ tel1::ura4$^+$/tel1::ura4+*
18		*pat1-114/pat1-114*
19	TT266	*h^-/h^- ade6-M216/ade6-M210 leu1-32/leu1-32 ura4-D18/ura4-D18*
20		*mek1(100)-9myc::LEU2/mek1(100)-9myc::LEU2 rec12::ura4$^+$/rec12::ura4+ pat1-114/pat1-114*
21	TT608	*h^- ade6-M216 leu1-32 ura4-D18 mek1(100)-9myc::LEU2 pat1-114*
22	TT305	*h^-/h^- ade6-M216/ade6-M210 leu1-32/leu1-32 ura4-D18/ura4-D18*
23		*mek1-9myc::LEU2/mek1-9myc::LEU2 pat1-114/pat1-114*
24	TT273	*h^-/h^- ade6-M216/ade6-M210 leu1-32/leu1-32 ura4-D18/ura4-D18mek1::ura4$^+$/mek1::ura4$^+$*
25		*mek1-T15A-9myc::LEU2/mek11-T15A-9myc::LEU2 pat1-114/pat1-114*
26	TT230	*h^- ade6-M26 leu1-32 ura4-D18 mek1-9myc::LEU2*
27	TT231	*h^+ ade6-469 his2 leu1-32 ura4-D18 mek1-9myc::LEU2*
28	TT253	*h- ade6-M26 ura4-D18 mek1::ura4$^+$*
29	TT254	*h^+ ade6-469 his2 leu1-32 ura4-D18 mek1::ura4$^+$*
30	TT689	*h- ade6-M26 leu1-32 ura4-D18 mek1::ura4$^+$ mek1-S12A-9myc::LEU2*
31	TT690	*h^+ ade6-469 his2 leu1-32 ura4-D18 mek1::ura4$^+$ mek1-S12A-9myc::LEU2*
32	TT691	*h- ade6-M26 leu1-32 ura4-D18 mek1::ura4$^+$ mek1-S14A-9myc::LEU2*
33	TT692	*h^+ ade6-469 his2 leu1-32 ura4-D18 mek1::ura4$^+$ mek1-S14A-9myc::LEU2*
34	TT162	*h- ade6-M26 leu1-32 ura4-D18 mek1::ura4$^+$ mek1-T15A-9myc::LEU2*
35	TT163	*h^+ ade6-469 his2 leu1-32 ura4-D18 mek1::ura4$^+$ mek1-T15A-9myc::LEU2*
36	TT675	*h- ade6-M26 leu1-32 ura4-D18 mek1::ura4$^+$ mek1-S12AS14AT15A-9myc::LEU2*

1	TT676	*h$^+$ ade6-469 his2 leu1-32 ura4-D18 mek1::ura4$^+$ mek1-S12AS14AT15A-9myc::LEU2*
2	TT693	*h- ade6-M26 leu1-32 ura4-D18 mek1::ura4$^+$ mek1-S12AS14AT15A-FHAD-9myc::LEU2*
3	TT694	*h$^+$ ade6-469 his2 leu1-32 ura4-D18 mek1::ura4$^+$mek1-S12AS14AT15A-FHAD-9myc::LEU2*
4	TT164	*h- ade6-M26 leu1-32 ura4-D18 mek1::ura4$^+$+ mek1-FHAD-9myc::LEU2*
5	TT165	*h$^+$ ade6-469 his2 leu1-32 ura4-D18 mek1::ura4$^+$mek1-FHAD-9myc::LEU2*
6	TT677	*h$^-$ ade6-M26 leu1-32 ura4-D18 mek1-T318A-9myc::LEU2*
7	TT678	*h$^+$ ade6-469 his2 leu1-32 ura4-D18 mek1-T318A-9myc::LEU2*
8	TT679	*h$^-$ ade6-M26 leu1-32 ura4-D18 mek1-T322A-9myc::LEU2*
9	TT680	*h$^+$ ade6-469 his2 leu1-32 ura4-D18 mek1-T322A-9myc::LEU2*
10	TT681	*h$^-$ ade6-M26 leu1-32 ura4-D18 mek1- T318A T322A-9myc::LEU2*
11	TT682	*h$^+$ ade6-469 his2 leu1-32 ura4-D18 mek1-T318A T322A -9myc::LEU2*
12	TT591	*h$^-$ ade6-M26 leu1-32 ura4-D18 mek1-D281A-9myc::ura4$^+$*
13	TT592	*h$^+$ ade6-469 his2 leu1-32 ura4-D18 mek1- D281A-9myc::ura4$^+$*
14	TT464	*h$^-$/h$^-$ ade6-M216/ade6-M210 leu1-32/leu1-32 ura4-D18/ura4-D18 mek1::ura4$^+$/mek1::ura4$^+$*
15		*mus81-13myc::kanMx6/ mus81-13myc::kanMx6 pat1-114/pat1-114*
16	TT468	*h$^-$/h$^-$ ade6-M216/ade6-M210 leu1-32/leu1-32 ura4-D18/ura4-D18 cds1::ura4$^+$/cds1::ura4$^+$*
17		*mus81-13myc::kanMx6/ mus81-13myc::kanMx6 pat1-114/pat1-114*
18	TT4-5	*h$^+$ his2 leu1-32 ura4-D18 mek1::ura4$^+$*
19	TT10-1	*h$^-$ ade6-M216 ura4-D18 mek1::ura4$^+$*
20	TT11	*h$^-$ ade6-M216 ura4-D18 cds1::ura4$^+$*
21	TT12	*h$^+$ leu1-32 his2 ura4-D18 cds1::ura4$^+$*
22	TT28	*h$^-$ ade6-M216 ura4-D18 mek1::ura4$^+$ cds1::ura4$^+$*
23	TT29	*h$^+$ leu1-32 his2 ura4-D18 mek1::ura4$^+$ cds1::ura4$^+$*
24	TT526	*h$^-$/h$^-$ ade6-M216/ade6-M210 leu1-32/leu1-32 ura4-D18/ura4-D18*
25		*mek1-T15A/KD-9myc::LEU2/mek1-T15A/KD-9myc::LEU2 pat1-114/pat1-114*
26	TT540	*h$^-$/h$^-$ ade6-M216/ade6-M210 leu1-32/leu1-32 ura4-D18/ura4-D18 mek1::ura4$^+$/mek1::ura4$^+$*
27		*mek1-T15A-9myc::LEU2/mek11-T15A-9myc::LEU2hsk1-3ha::ura4$^+$/hsk1-3ha:: ura4$^+$ pat1-114/pat1-114*
28	TT277	*h$^-$/h$^-$ ade6-M216/ade6-M210 leu1-32/leu1-32 ura4-D18/ura4-D18*
29		*mek1-FHAD-9myc::LEU2/mek1-FHAD-9myc::LEU2 pat1-114/pat1-114*
30	TT548	*h$^-$/h$^-$ ade6-M216/ade6-M210 leu1-32/leu1-32 ura4-D18/ura4-D18*
31		*mek1-T15A/FHAD-9myc::LEU2/mek1-T15A/FHAD-9myc::LEU2 pat1-114/pat1-114*
32	TT168	*h$^-$ ura4-D18 mek1::ura4$^+$ cdc12 lys3*
33	TT166	*h$^-$ leu1-32 ura4-D18 mek1::ura4$^+$ mek1-T15A-9myc::LEU2 cdc12 lys3*
34	TT159	*h$^+$ his2 leu1-32 ura4-D18 mek1::ura4$^+$ mek1-T15A-9myc::LEU2*
35	TT167	*h$^-$ leu1-32 ura4-D18 mek1::ura4$^+$ mek1-FHAD-9myc::LEU2 cdc12 lys3*
36	TT160	*h$^+$ his2 leu1-32 ura4-D18 mek1::ura4$^+$ mek1-FHAD-9myc::LEU2*

1	TT545	*h$^-$ leu1-32 ura4-D18 mek1::ura4$^+$ mek1-T15A/FHAD-9myc::LEU2 cdc12 lys3*
2	TT538	*h$^+$ his2 leu1-32 ura4-D18 mek1::ura4$^+$ mek1-T15A/FHAD-9myc::LEU2*
3	TT390	*h$^-$ ura4-D18 mek1-KD-9myc::ura4$^+$ cdc12 lys3*
4	TT177	*h$^+$ his2 leu1-32 ura4-D18 mek1-KD-9myc::ura4$^+$*
5	TT493	*h$^-$ leu1-32 ura4-D18 mek1::ura4$^+$ mek1-T15A/KD-9myc::LEU2 cdc12 lys3*
6	TT494	*h$^+$ his2 leu1-32 ura4-D18 mek1::ura4$^+$ mek1-T15A/KD-9myc::LEU2*
7	TT253	*h$^-$ ade6-M26 ura4-D18 mek1::ura4$^+$*
8	TT254	*h$^+$ ade6-469 his2 leu1-32 ura4-D18 mek1::ura4$^+$*
9	TT162	*h$^-$ ade6-M26 leu1-32 ura4-D18 mek1::ura4$^+$ mek1-T15A-9myc::LEU2*
10	TT163	*h$^+$ ade6-469 his2 leu1-32 ura4-D18 mek1::ura4$^+$ mek1-T15A-9myc::LEU2*
11	TT164	*h$^-$ ade6-M26 leu1-32 ura4-D18 mek1::ura4$^+$ mek1-FHAD-9myc::LEU2*
12	TT165	*h$^+$ ade6-469 his2 leu1-32 ura4-D18 mek1::ura4$^+$ mek1-FHAD-9myc::LEU2*
13	TT541	*h$^-$ ade6-M26 leu1-32 ura4-D18 mek1::ura4$^+$ mek1-T15A/FHAD-9myc::LEU2*
14	TT542	*h$^+$ ade6-469 his2 leu1-32 ura4-D18 mek1::ura4$^+$ mek1-T15A/FHAD-9myc::LEU2*
15	TT188	*h$^-$ ade6-M26 ura4-D18 mek1-KD-9myc::ura4$^+$*
16	TT189	*h$^+$ ade6-469 his2 leu1-32 ura4-D18 mek1-KD-9myc::ura4$^+$*
17	TT475	*h$^-$ ade6-M26 leu1-32 ura4-D18 mek1::ura4$^+$ mek1-T15A/KD-9myc::LEU2*
18	TT476	*h$^+$ ade6-469 his2 leu1-32 ura4-D18 mek1::ura4$^+$ mek1-T15A/KD-9myc::LEU2*
19	TT551	*h$^{-/}$h$^-$ ade6-M216/ade6-M210 leu1-32/leu1-32 ura4-D18/ura4-D18 mek1-9myc::LEU2/mek1-9myc::LEU2*
20		*rad3::ura4$^+$/rad3::ura4$^+$ pat1-114/pat1-114*
21	TT552	*h$^{-/}$h$^-$ ade6-M216/ade6-M210 leu1-32/leu1-32 ura4-D18/ura4-D18 mek1-9myc::LEU2/mek1-9myc::LEU2*
22		*tel1:: ura4$^+$/tel1::ura4$^+$ pat1-114/pat1-114*
23	TT553	*h$^{-/}$h$^-$ ade6-M216/ade6-M210 leu1-32/leu1-32 ura4-D18/ura4-D18 mek1-9myc::LEU2/mek1-9myc::LEU2*
24		*rad3::ura4$^+$/rad3::ura4$^+$ tel1::ura4$^+$/tel1::ura4$^+$ pat1-114/pat1-114*
25	TT305	*h$^{-/}$h$^-$ ade6-M216/ade6-M210 leu1-32/leu1-32 ura4-D18/ura4-D18 mek1-9myc::LEU2/mek1-9myc::LEU2*
26		*pat1-114/pat1-114*
27		

28

29 Strains indicated by a, b and c superscripts were previously described (24, 34, 35).
30 Other strains were constructed in this study.

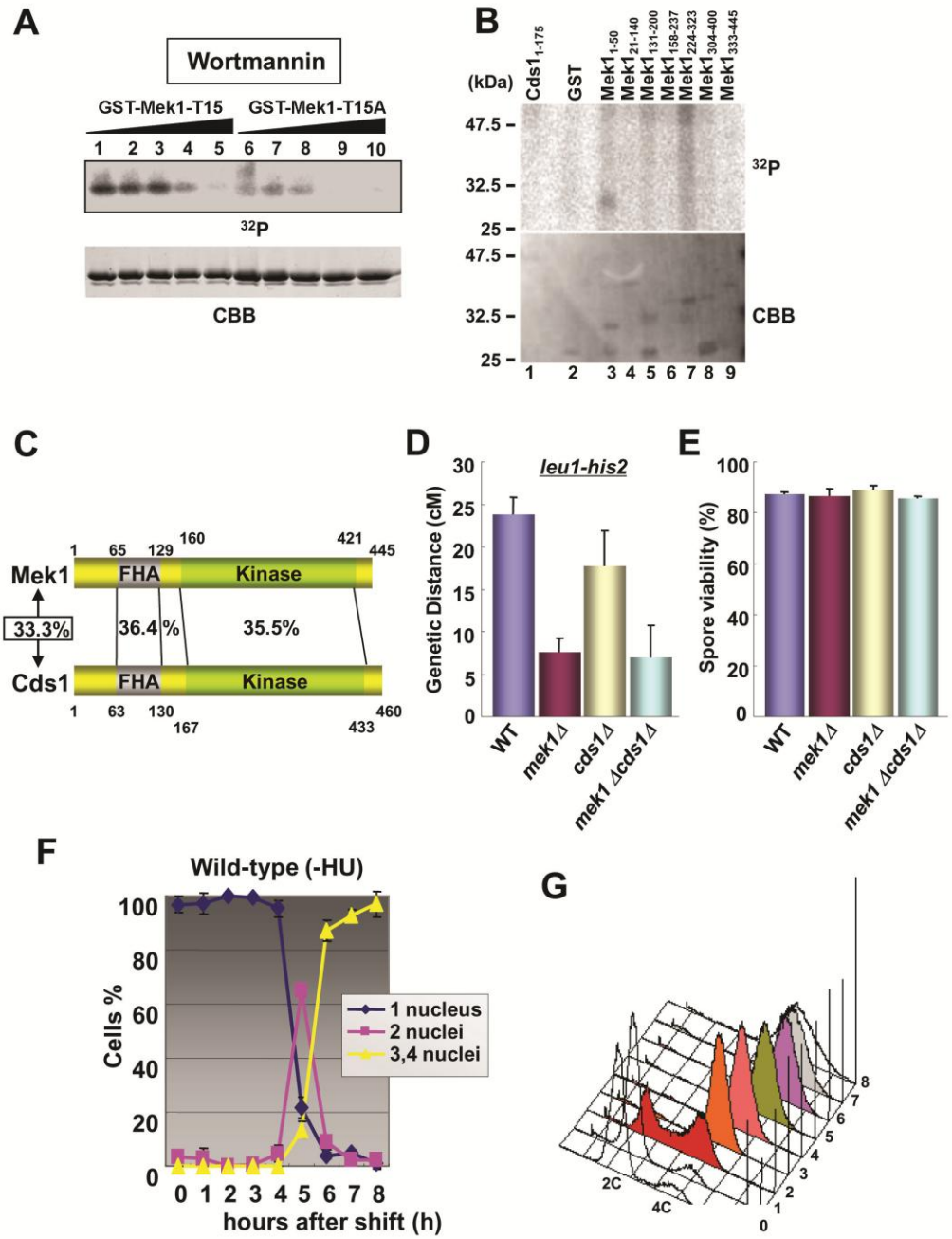

Figure S1. Properties of Mek1 and Cds1 kinases. (A) Wortmannin, an inhibitor of Rad3 kinase activity, blocks ^{32}P incorporation into the GST-Mek1-T15 (lanes 1–5) and GST-Mek1-T15A (lanes 6–10) fragments in proportion to its increasing amounts in the reaction mixture of the Rad3 kinase assay. Proteins were separated by SDS-PAGE. ^{32}P incorporation is shown in the upper panel (^{32}P), and the amount of loaded protein assessed by CBB staining is shown in the lower panel (CBB). ^{32}P incorporation was visualized using a phosphor image analyzer (Fuji Film, Tokyo, Japan). (B) Affinity purified GST-Rad3 kinase from fission yeast was incubated with [g-^{32}P]ATP and GST-Cds1$_{1-175}$, GST, GST-Mek1$_{1-50}$, GST-Mek1$_{21-140}$, GST-Mek1$_{131-200}$, GST-Mek1$_{158-237}$, GST-Mek1$_{224-323}$, GST-Mek1$_{304-400}$ and GST-Mek1$_{333-445}$ substrates. Almost equal amounts of loaded Mek1 substrates were confirmed by CBB staining. (C) Comparison of domain structures between Mek1 and Cds1 of *S. pombe*. Similar amounts of whole protein (33.3%), FHA domain (36.4%), and kinase domain (35.5%) are highlighted. (D) Intergenic recombination rates between *leu1* and *his2* genes on chromosome I were examined in WT (NP32-2A x NP16-6B), *mek1Δ* (TT4-5 x TT10-1), *cds1Δ* (TT11 x TT12), and *mek1Δ cds1Δ* (TT28 x TT29) strains. The data shown are the average of three independent experiments with standard errors (error bars). (E) Spore viability was examined in the denoted strains. The data shown are the averages of three independent experiments with standard errors (error bars). (F) Measurements of the change in nuclear number allowed for monitoring the successful meiotic progression of *mek1-9myc pat1* cells (TT305). (G) Progression of meiotic S phase was monitored by FACS analysis of DNA content.

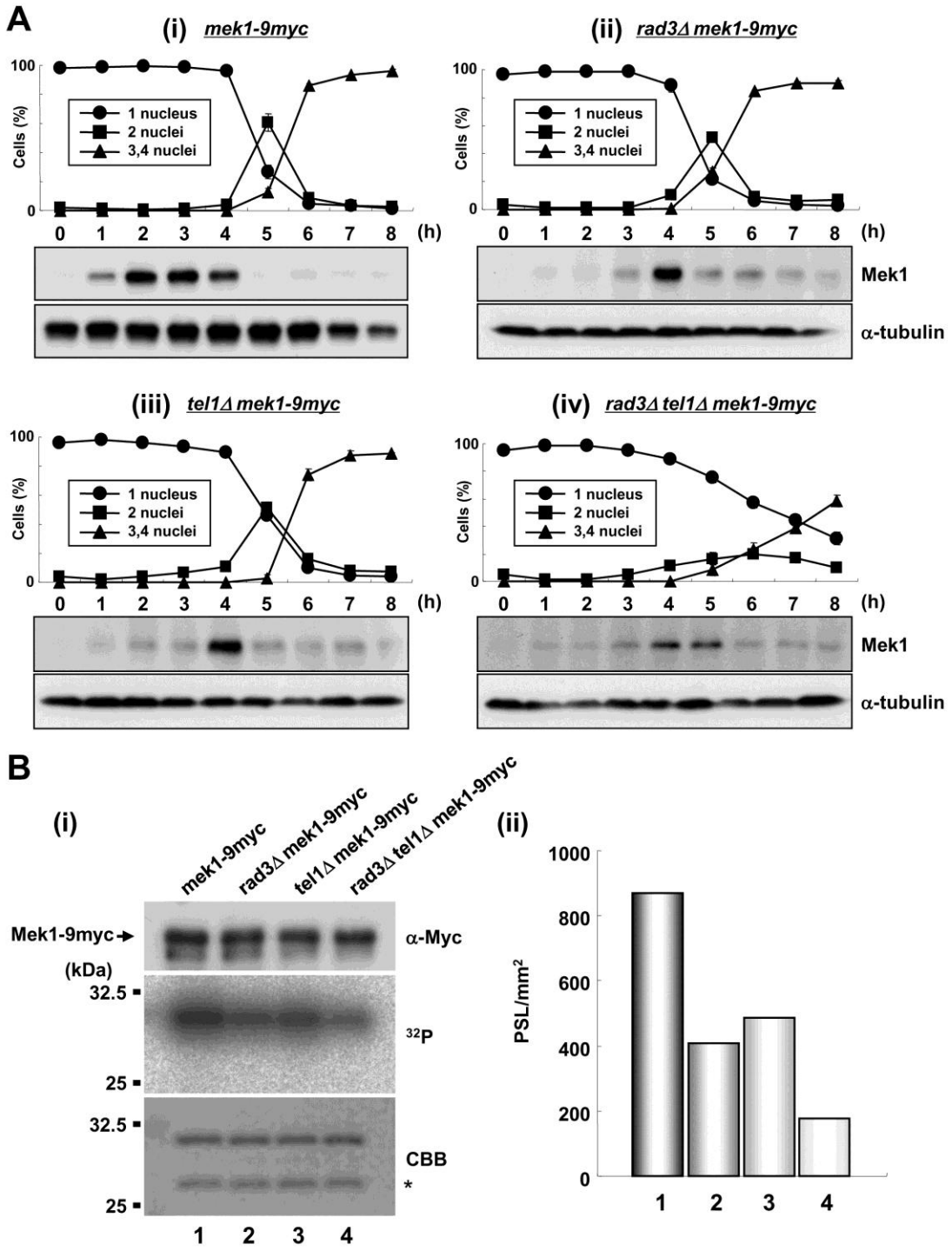

Figure S2. Kinase activity of Mek1 partially depends on Rad3 and Tel1 during meiosis. (A) The following strains were induced to enter meiosis by a temperature shift: (i) *mek1-9myc pat1* (TT305), (ii) *rad3Δ mek1-9myc pat1* (TT551), (iii) *tel1Δ mek1-9myc pat1* (TT552), and (iv) *rad3Δ tel1Δ mek1-9myc pat1* (TT553). Changes in nuclear number were monitored. The data are the mean ± SD of at least three independent experiments. Protein samples were taken after the temperature shift at the indicated time points and western blot analysis was performed to detect Mek1-9myc (Mek1). α-Tubulin was used as a loading control. (B) Detection of the kinase activity of Mek1 *in vivo*. Mek1 kinases were prepared by immunoprecipitation from protein extracts 4 h after the temperature shift, and kinase activities were measured using the AL fragment as a substrate. (i) The amount of Mek1 kinase immunoprecipitates as assessed by western analysis with the anti-Myc antibody, incorporation of ^{32}P into the substrate, and the amount of loaded protein as assessed by CBB staining are shown in the upper, middle and lower panels, respectively. Asterisk indicates the putative degradation product. (ii) The intensities of the phosphorylated bands in B (i) were measured by a densitometer and are presented as bar graphs.

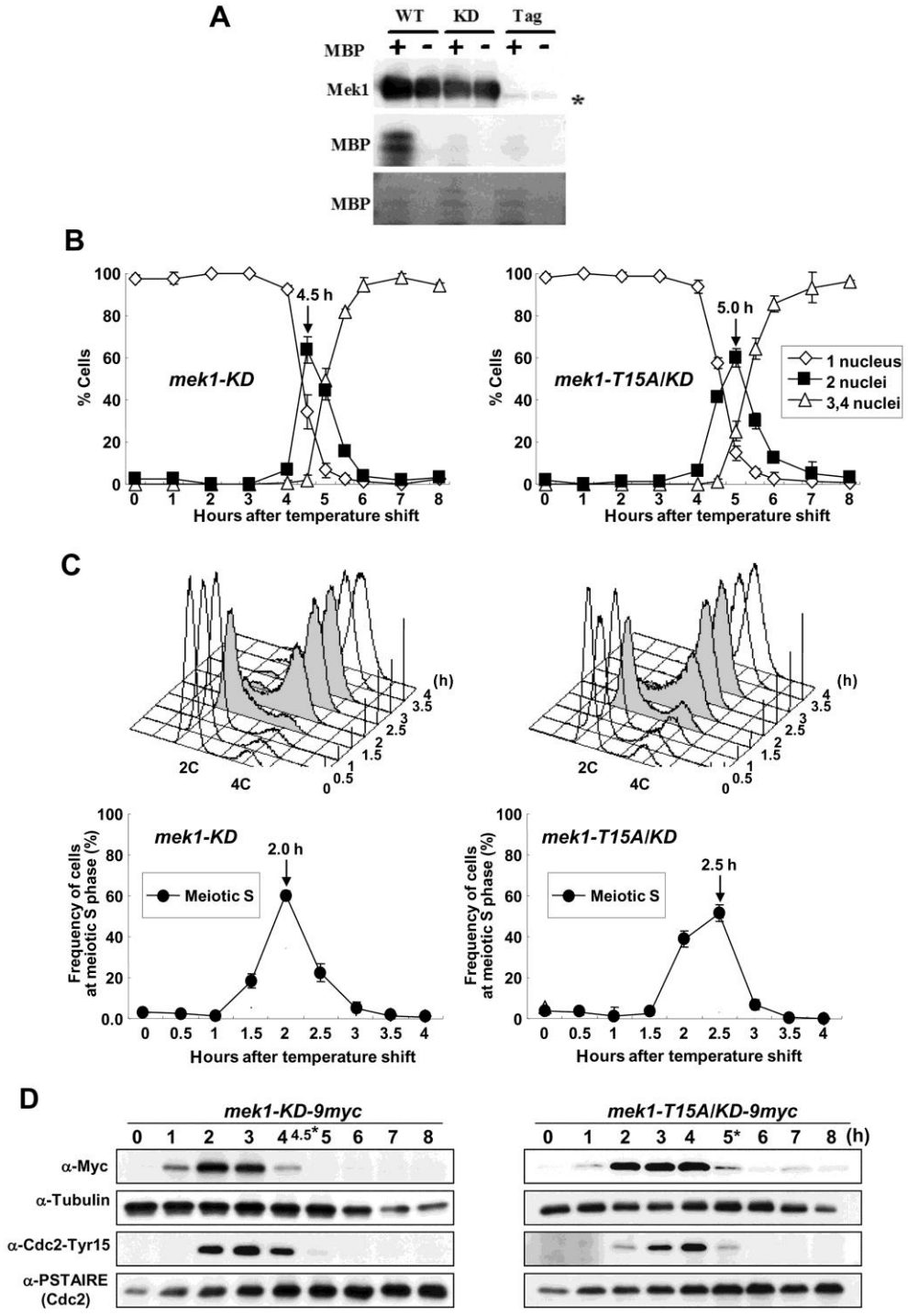

Figure S3. Meiotic delay in *mek1-T15A-9myc pat1* cells is partially suppressed by the *KD* mutation. (A) An *in vitro* kinase assay shows that the Mek1-KD protein lacks kinase activity. MBP was used as a substrate. An asterisk indicates the heavy chain of the antibody used to precipitate Mek1 for the assay (see Materials and Methods). (B) Meiotic progression was monitored following the induction of meiosis at the indicated times in *mek1*$^{+}$, *mek1-KD-9myc pat1* (GP21), and *mek1-T15A/KD-9myc pat1* cells (TT526). (These strains are used in B and C). Changes in nuclear number were monitored. (C) Progression of meiotic S phase was monitored by FACS analysis of DNA content (upper panel) and evaluated by Modfit LT software to determine the fraction of cells undergoing DNA replication at each time point (lower panel). The data in B and C are the mean ± SD of at least three independent experiments. (D) Samples were taken after the temperature shift at the indicated times and western blot analysis was performed to detect Mek1-9myc, α-tubulin, Tyr15-phosphorylated Cdc2, and total Cdc2. Tubulin was used as a loading control. Asterisks show the times when the frequency of cells having two nuclei peaked.

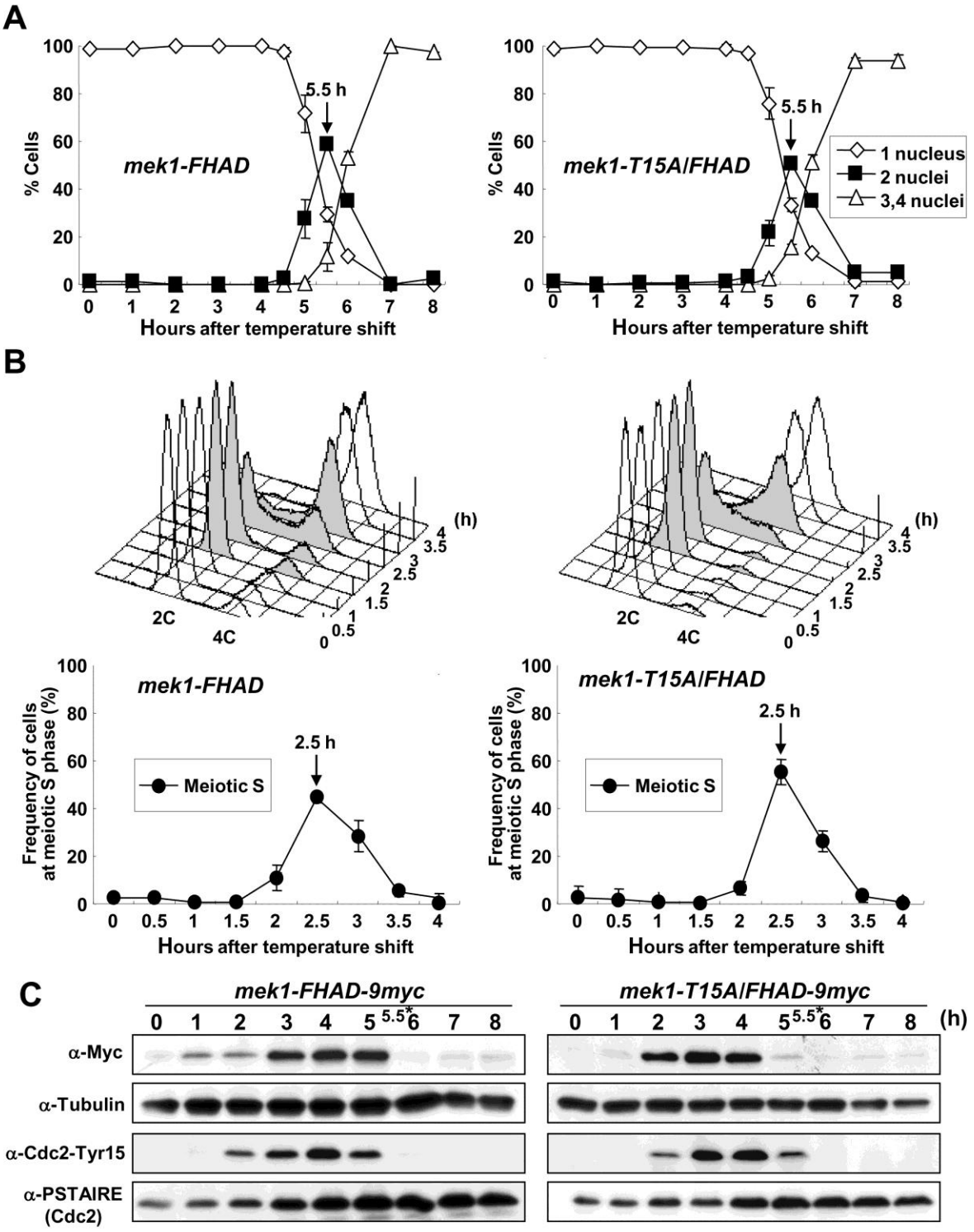

Figure S4. Meiotic delay in *mek1-T15A-9myc pat1* cells is partially suppressed by the *FHAD* mutation. *mek1-FHAD-9myc pat1* (TT277), *mek1-T15A/FHAD-9myc pat1* (TT548), *mek1-KD-9myc pat1* (GP21), and *mek1-T15A/KD-9myc pat1* (TT526) cells were induced to undergo meiosis, as shown in Figure 2. The data are the mean ± SD of at least three independent experiments. (A) Changes in the numbers of nuclei per cell. (B) Progression of meiotic S phase was monitored by FACS analysis of DNA content (upper panels) and evaluated by Modfit LT software to determine the fraction of cells undergoing DNA replication at each time point (lower panels). (C) Samples were taken after the temperature shift at the indicated times and western blot analysis was performed to detect Mek1-9myc, α-tubulin, Tyr15-phosphorylated Cdc2, and total Cdc2. Tubulin was used as a loading control. Asterisks indicate the peaks of the two-nucleus cell populations.

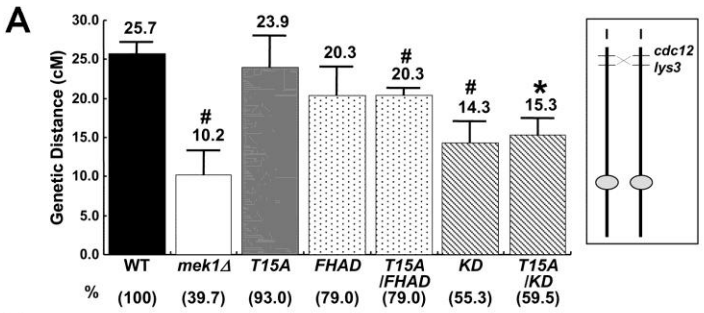

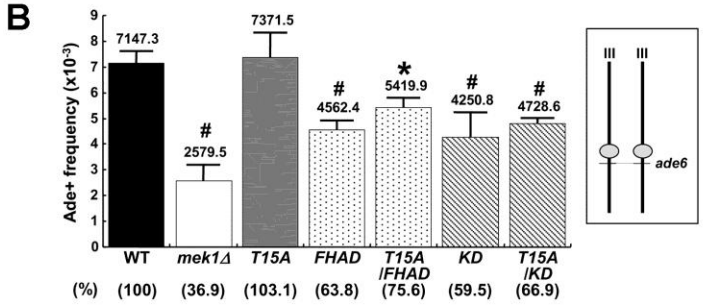

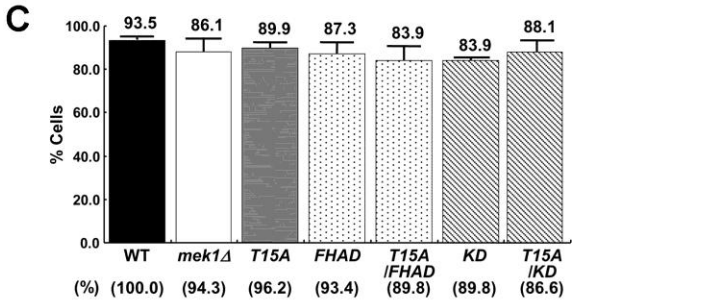

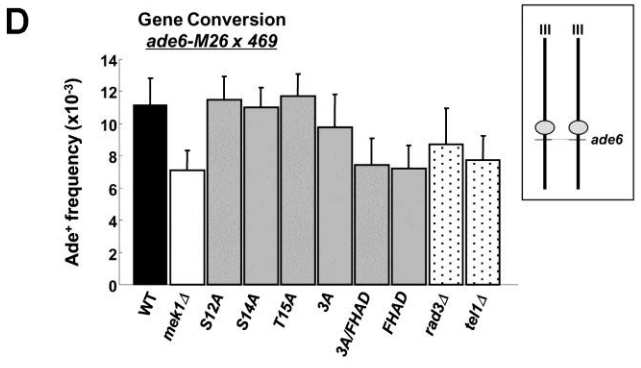

E

	mek1 genotype	Δ	KD	T15A	FD	15A/KD	15A/FD
Phenotype	Meiotic delay (min)	0	~30	60	30	0	30
	Meiotic S (min)	0	0	60	30	30	30
	Recombination	+++	++	-	+	++	+

Δ = *mek1*Δ, K1D= *mek1-KD*, T15A= *mek1-T15A*, FD= *mek1-FHAD*, 15A/KD=*mek-T15A/KD*, 15A/FD=*mek-T15A/FHAD*

Figure S5. Recombination frequencies are reduced in *mek1-KD-9myc* and *mek1-FHAD-9myc* cells, but not in *mek1-T15A-9myc* cells. The data presented are the mean ± SD of at least three independent experiments. The means are shown above each bar. The chromosomal positions of the loci and centromeres (gray balls) are illustrated in the insets of (A) and (B) (right). Numbers below histograms show responses normalized to that of wild-type cells. (A) Frequency of intergenic recombination between *cdc12*$^+$ and *lys3*$^+$ on chromosome I. At least 100 tetrads were analyzed in each experiment. Only those that generated four viable spores were used to calculate genetic distances (cM). The strains used were wild type (NP32-2B x NP32-2A), *mek1Δ* (TT168 x TT4-5), *mek1-T15A-9myc* (TT166 x TT159), *mek1-FHAD-9myc* (TT167 x TT160), *mek1-T15A/FHAD-9myc* (TT545 x TT538), *mek1-KD-9myc* (TT390 x TT177), and *mek1-T15A/KD-9myc* (TT493 x TT494). All measurements except for T15A and FHAD mutants are statistically significant when WT and denoted strains are compared (* = P<0.01; # = P<0.05). (B) Frequency of intragenic recombination between the *ade6-M26* and *ade6-469* alleles on chromosome III. The strains used were wild-type (TT230 x MS105-1B), *mek1Δ* (TT253 x TT254), *mek1-T15A-9myc* (TT162 x TT163), *mek1-FHAD-9myc* (TT164 x TT165), *mek1-T15A/FHAD-9myc* (TT541 x TT542), *mek1-KD-9myc* (TT188 x TT189), and *mek1-T15A/KD-9myc* (TT 475 x TT 476). All measurements except for T15A mutant are statistically significant when WT and denoted strains are compared (* = P<0.01; # = P<0.05). (C) Spore viability. Tetrads were dissected with a micromanipulator and cultured on sporulation medium, and viability was assessed after 3–4 d. The strains used were the same as those used in the intragenic recombination assays (B). (D) Intragenic recombination rates between *ade6-M26* and *ade6-469* on chromosome III were examined in the indicated strains. The data presented are the mean ± SD of at least three independent experiments. The chromosomal positions of the loci and centromeres (shown by gray balls) are illustrated in the right panel. (E) Summary of the phenotypes of *mek1* mutants. Numbers represent the time (min) of delay in meiotic progression and initiation of meiotic S phase. Symbols (+++, ++ and +) denote the largely reduced, reduced and modestly reduced recombination frequencies. A symbol (-) signifies that the recombination frequency is similar to that of WT cells.

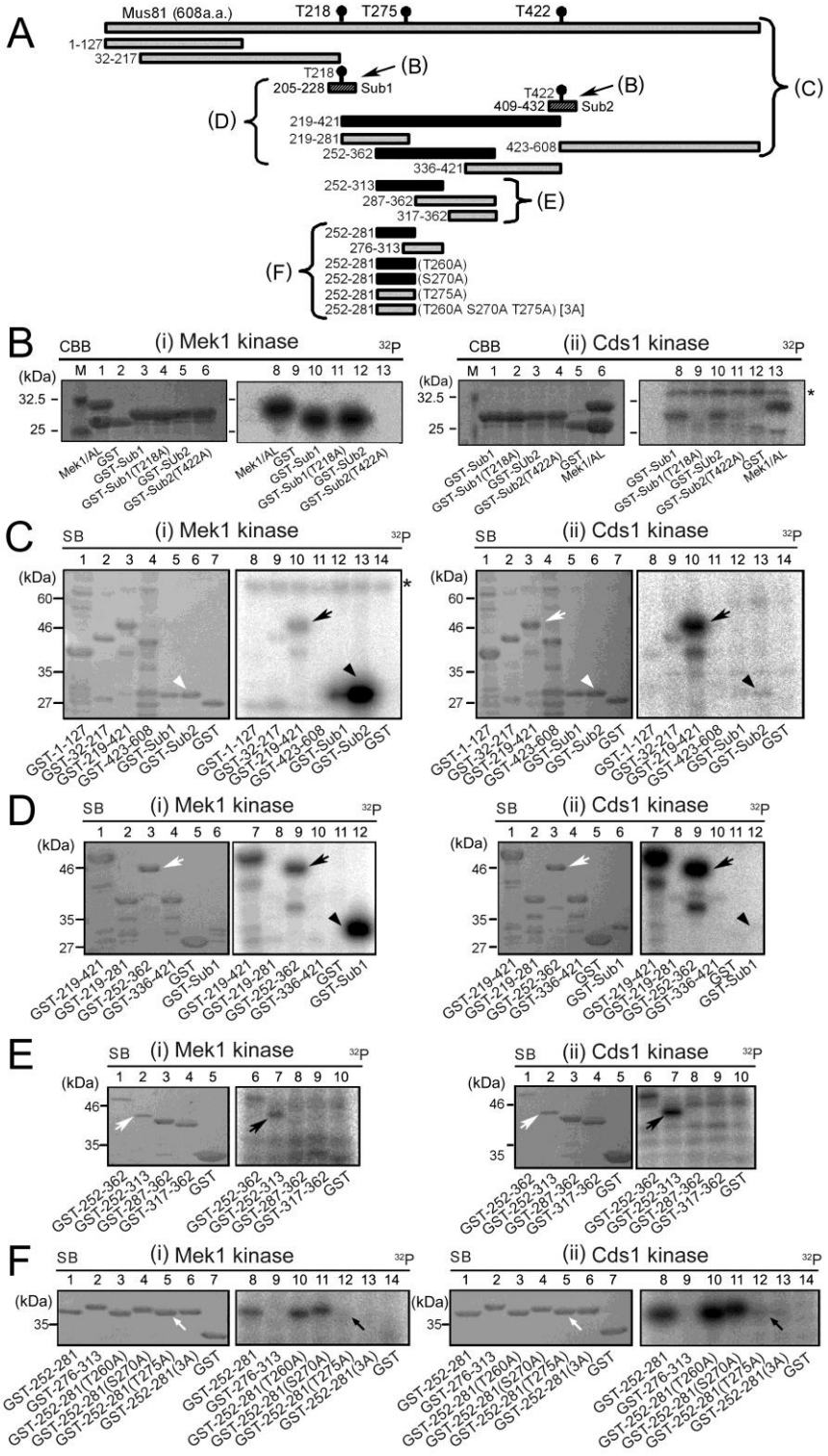

Figure S6. Mek1 phosphorylates Mus81 *in vitro*. (A) Mek1 kinase, but not the Mek1-KD form, prepared from mitotic cells phosphorylates Mus81 *in vitro*. (i) Equal amounts of extracts obtained from logarithmically growing *S. pombe* cells that exogenously expressed Mek1-9Myc or Mek1-KD-9Myc proteins were immunoprecipitated and immunoblotted with the anti-Myc antibody (PL14). (ii) Immunoprecipitates were used for the *in vitro* kinase assay with GST-Mus81 and GST alone (negative control) as substrates. The asterisk indicates a putative degraded band. (B) Mek1 kinase activity in immunoprecipitates of meiotic *S. pombe* cells phosphorylates Mus81 *in vitro*. (i) Expression pattern of 9Myc-Mek1 during meiosis (from 0 to 7 h after nitrogen starvation) was monitored by western blot analysis using the anti-Myc antibody. Expression of a-tubulin was also monitored as a loading control. (ii) Mek1 kinase assay *in vitro* using immunoprecipitates prepared from meiotic cell extracts with the anti-Myc antibody as a kinase. The Mek1 AL fragment (positive control), GST-Mus81, and GST alone (negative control) were used as substrates (arrows). The panels at the top show the autophosphorylation of Mek1. The asterisk indicates putative degraded or non-specific bands.

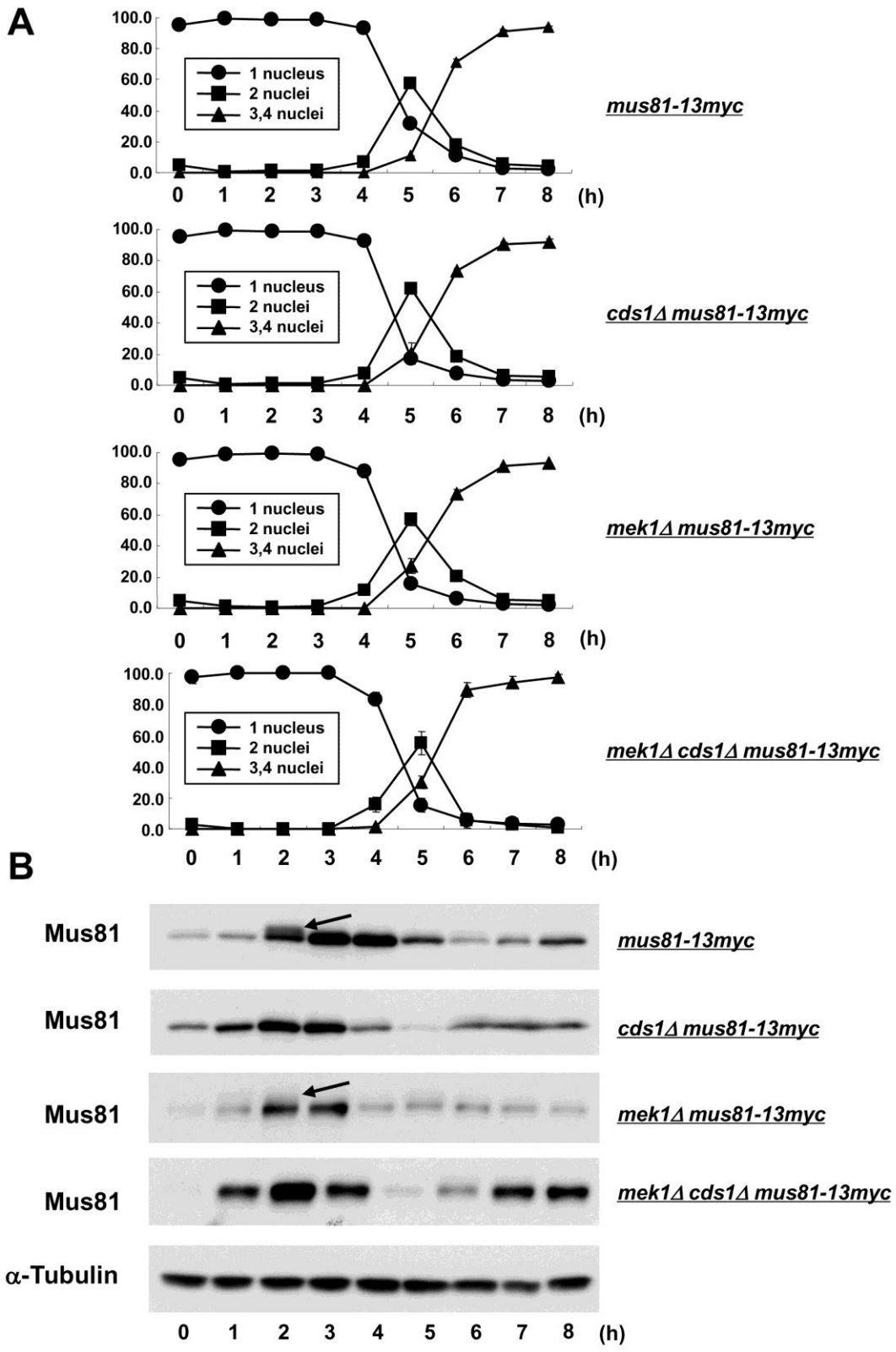

Figure S7. Meiotic progression and western blot analyses of *mus81*-related *S. pombe* cells. (A) Meiotic progression was monitored following induction of meiosis at the indicated times for the denoted *S. pombe* cells. (B) Western blot analysis of protein samples that were taken after the temperature shift at the indicated time points using the anti-Myc antibody to detect Mus81-9Myc. α-Tubulin was used as a loading control. Arrows indicate the putative phosphorylated bands of Mus81.

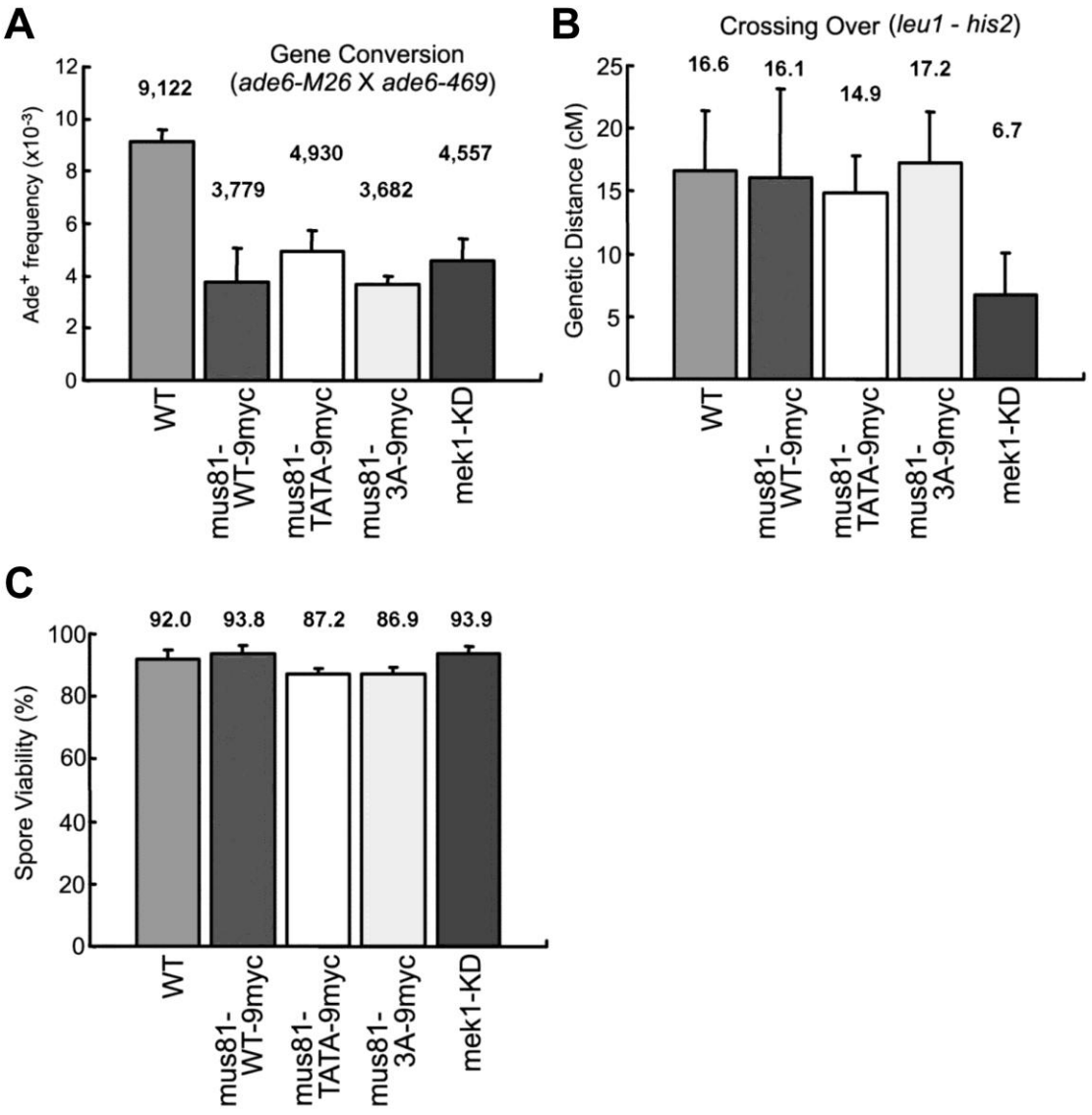

Figure S8. The recombination frequency, spore viability and UV sensitivity of *mus81* mutants. The data presented are the mean ± SD of at least three independent experiments. The mean values are shown above each bar. At least 100 tetrads were analyzed in each experiment. (A) Frequency of intragenic recombination between *ade6-M26* and *ade6-469* on chromosome III of the denoted *S. pombe* cells. (B) Frequency of intergenic recombination between *leu1*$^+$ and *his2*$^+$ on chromosome II. Only tetrads that generated four viable spores were used to calculate the genetic distance (cM). (C) Spore viability of denoted *S. pombe* cells. Tetrads were dissected by the micromanipulator and cultured on sporulation medium, and viability was assessed after 3–4 d.

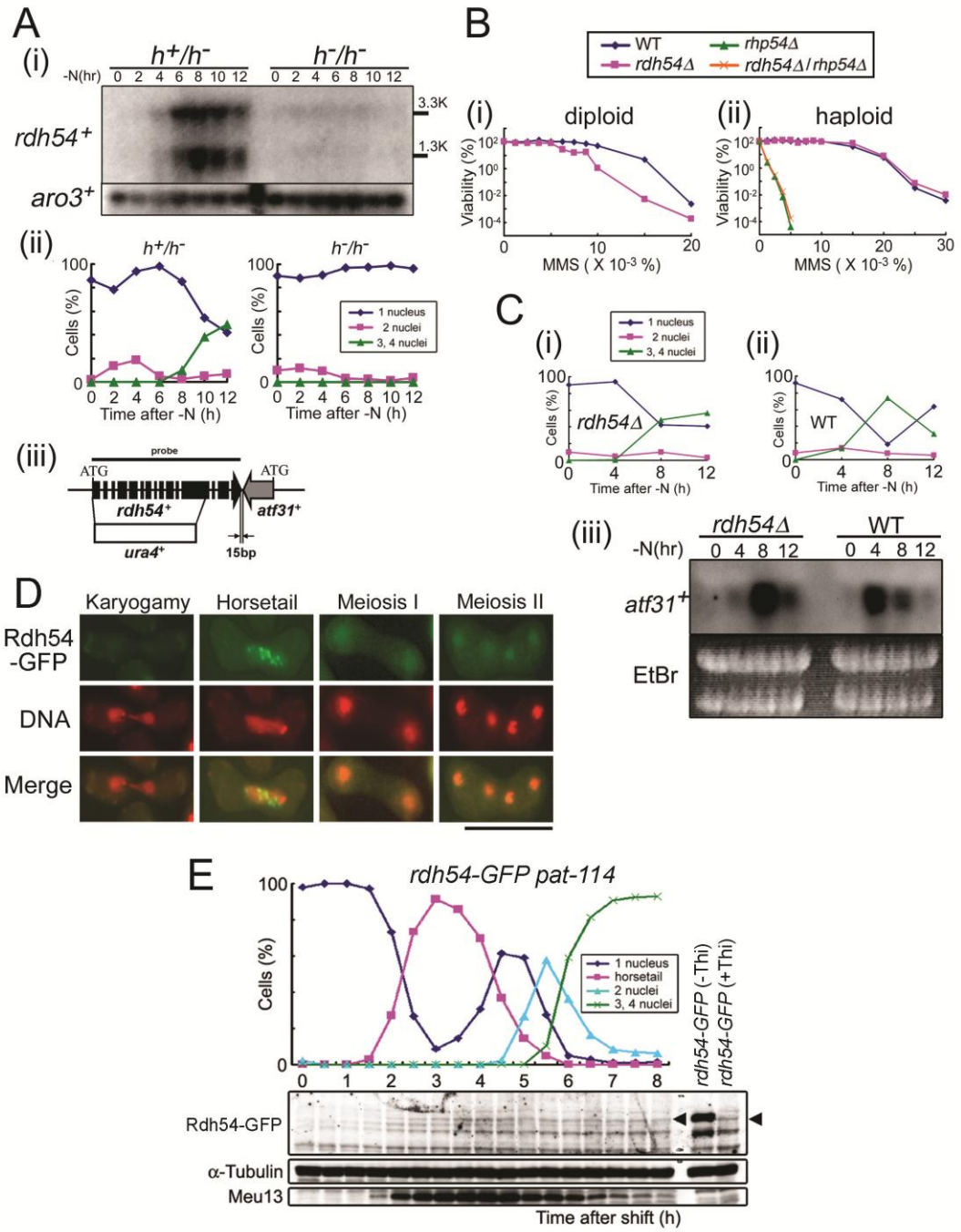

Figure S9. Meiotic expression of *rdh54*$^+$ and subcellular localization of Rdh54-GFP. (A) Northern blot analysis of *rdh54*$^+$ and *aro3*$^+$ (loading control) expression during meiosis. (i) Total RNA was extracted from diploid *h*$^+$/*h*$^-$ (CD16-1) and *h*$^-$/*h*$^-$ (CD16-5) cells at the indicated times after nitrogen starvation, which causes the CD16-1, but not the CD16-5, cells to enter meiosis. The RNA of these cells was blotted and probed with the protein-coding regions of the *rdh54*$^+$ and *aro3*$^+$ genes. (ii) Meiotic profiles of the cells used for RNA extraction. The frequency of Hoechst 33342-stained cells with one, two, three, or four nuclei was assessed by counting at least 200 cells under a microscope at 2-h intervals. (iii) The structure of the *rdh54*$^+$ gene and its surrounding regions. The *rdh54*$^+$ gene consists of fifteen exons, which are shown as filled boxes. The *rdh54*$^+$ and *atf31*$^+$ genes are transcribed in the opposite direction, and their termination codons are separated by only 15 bp. To disrupt the *rdh54*$^+$ gene, its initiation codon through to the twelfth exon was replaced with the *ura4*$^+$. The region that was deleted from *rdh54*$^+$ in the process is indicated by the white box. (B) The MMS sensitivity of diploid and haploid *rdh54Δ* cells. Diploid (i) or haploid (ii) cells grown to the mid-log phase were spread on YPD plates containing various concentrations of MMS and incubated at 30°C for four days. (C) Expression of *atf31*$^+$ in *rdh54Δ* cells. (i) Total RNA was extracted from *rdh54Δ* (TK18-A x TK18-D) and WT (TP4-5A x TP4-1D) cells at the indicated times after meiosis was induced by nitrogen starvation. The graphs show the meiotic profiles of the cells used for RNA extraction. The frequency of Hoechst 33342-stained cells with one, two, three, or four nuclei was assessed by counting at least 200 cells under a microscope. (ii) The extracted RNA was subjected to northern blot analysis using a probe based on the protein-coding region of the *atf31*$^+$ gene to detect the *atf31*$^+$ transcript alone. (D) Live observation of Rdh54-GFP during meiosis (karyogamy, horsetail, meiosis I and meiosis II). The *h*^{90}*rdh54-GFP* (TK-123) cells induced to meiosis were analyzed by fluorescence microscopy for DNA (red) and Rdh54-GFP (green). The merged images of the two signals are indicated in the lowermost panels. Bar, 10 mm. (E) Western blot analysis of Rdh54-GFP protein expression during meiosis. Cells of the *rdh54-GFP pat1-1* strain (TK-128) were induced to enter synchronous meiosis, and cell extracts were prepared every 30 min. Cells of the TP4-5A strain expressing Rdh54-GFP under the control of the *nmt41* promoter were grown in the presence (+Thi) or absence (-Thi) of thiamine, and cell extracts were prepared. These extracts were dissolved in HB buffer and subjected to western blot analysis using antibodies against GFP, α-Tubulin and Meu13. α-Tubulin and Meu13 were used as loading controls and a meiotic timing control, respectively. The arrowhead indicates the band for Rdh54-GFP.

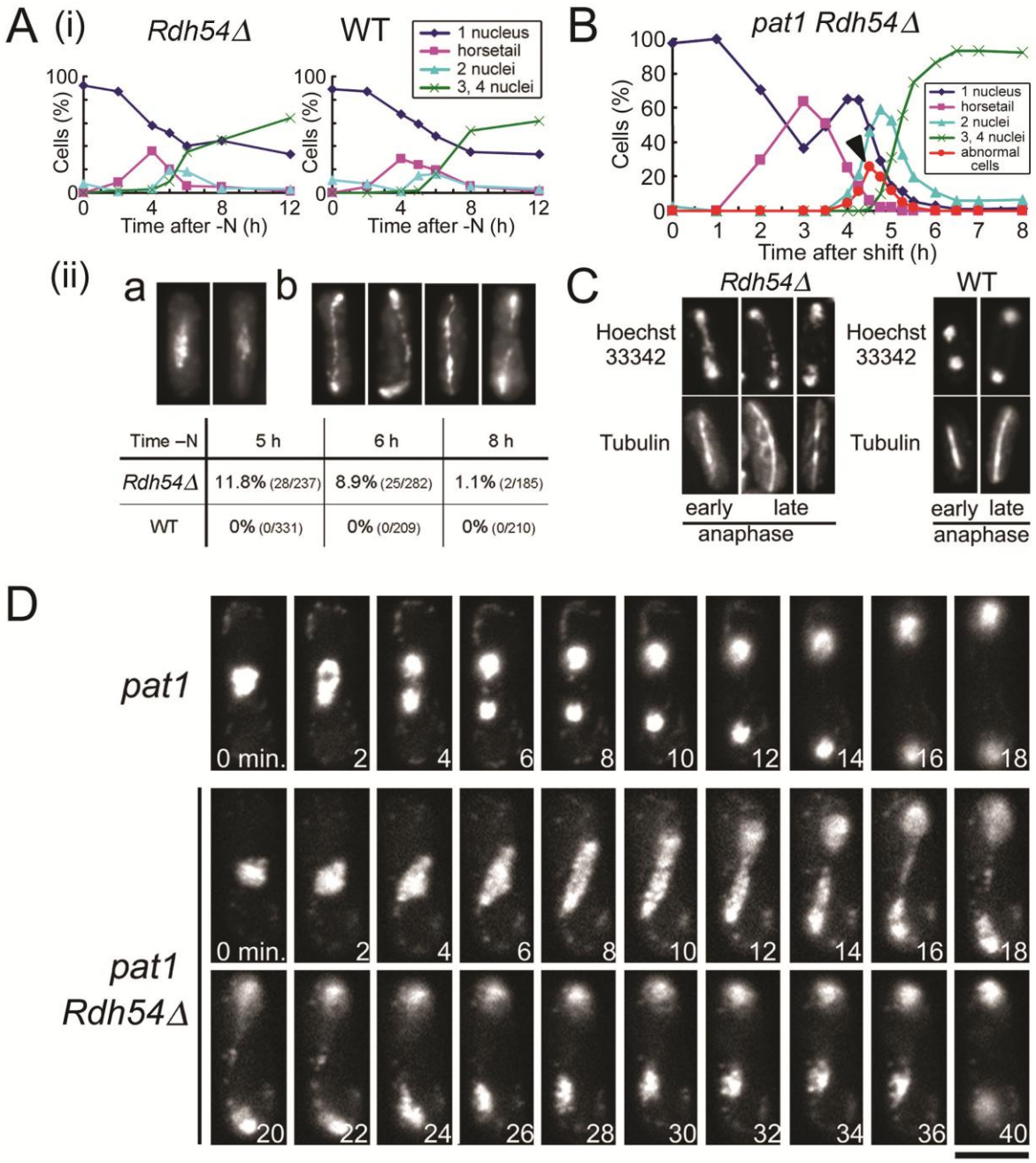

Figure S10. Meiotic nuclear morphology of *rdh54Δ* cells. (A) *rdh54Δ* (TK18-A x TK18-D) and WT (TP4-5A x TP4-1D) cells were induced to enter meiosis by nitrogen starvation and their nuclear phenotypes were examined. (i) The graphs depict the meiotic profiles of cells used for the microscopic observations. Frequencies of Hoechst 33342-stained cells with one, two, three, or four nuclei were assessed by counting at least 200 cells under a microscope. (ii) Abnormal nuclear morphology observed in meiotic *rdh54Δ* cells. Typical images of the anomalous granule-like structures within a single nuclei (a) and the abnormal separation of the two nuclei (b) at meiosis I in *rdh54Δ* cells. The percentage of cells harboring these abnormal nuclei at 5, 6, and 8 hours are summarized in the table shown below. (B) Homozygous diploid *pat1rdh54Δ* cells (TK29) were cultured to the mid-log phase, transferred to EMM-N medium for 16 h at 25°C, and then shifted to 34°C to inactivate Pat1 and to synchronize meiosis. The progression of meiosis was monitored by Hoechst 33342 staining of samples that were collected every 15 min, 30 min, or 1 h after the temperature shift. At least 150 cells were scored by fluorescence microscopy for each time point. An arrowhead shows when the frequency of abnormal cells peaked. (C) Chromosomal DNA and microtubules in *rdh54Δ* (TK18-A x TK18-D) and WT (TP4-5A x TP4-1D) cells were stained by Hoechst 33342 and the anti-a-tubulin antibody TAT-1, respectively. (D) Abnormal morphology and aberrant separation of nuclei during meiosis I in live meiotic *pat1 rdh54Δ* cells as revealed by time-lapse photography. The images of the *pat1* strain are shown as a control. The nuclei of *pat1* (JZ670) and *pat1 rdh54Δ* (TK29) cells were stained by Hoechst 33342, and images were recorded at 2-min intervals until the nuclei were completely segregated. Bar, 5 mm.

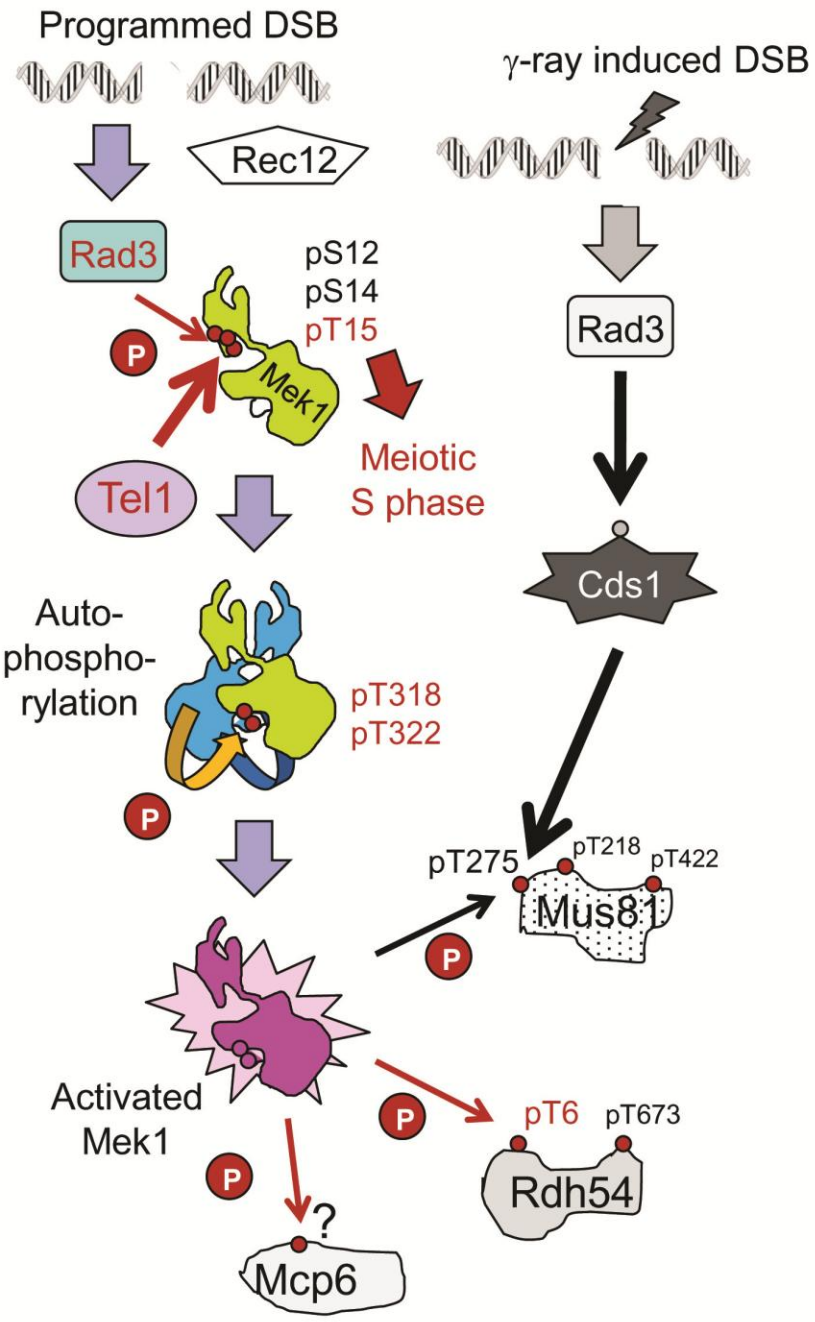

Figure S11. The signal transduction cascade of meiotic progression identified in this study (colored). Protein kinases and their phosphorylation targets are shown by red balls with residue numbers. Some residues are numbered in small fonts because their physiological significance remains unclear.